

Locating and Editing Factual Knowledge in GPT

Kevin Meng ^{*1} David Bau ^{*2} Alex Andonian ¹ Yonatan Belinkov ³

Abstract

We investigate the mechanisms underlying factual knowledge recall in autoregressive transformer language models. First, we develop a causal intervention for identifying neuron activations capable of altering a model’s factual predictions. Within large GPT-style models, this reveals two distinct sets of neurons that we hypothesize correspond to *knowing* an abstract fact and *saying* a concrete word, respectively. This insight inspires the development of ROME, a novel method for editing facts stored in model weights. For evaluation, we assemble COUNTERFACT, a dataset of over twenty thousand counterfactuals and tools to facilitate sensitive measurements of knowledge editing. Using COUNTERFACT, we confirm the distinction between saying and knowing neurons, and we find that ROME achieves state-of-the-art performance in knowledge editing compared to other methods. An interactive demo notebook, full code implementation, and the dataset are available at <https://rome.baulab.info/>.

1. Introduction

Knowing differs from *saying*: knowledge of a fact is different from uttering words by rote, because knowledge is consistent across syntactic variation (Elazar et al., 2021a). We ask if factual knowledge within GPT corresponds to a localized computation that can be edited.

Large language transformers have been observed to make predictions consistent with factual knowledge (Petroni et al., 2019; Jiang et al., 2020; Roberts et al., 2020; Brown et al., 2020), including both autoregressive GPT (Radford et al., 2019; Brown et al., 2020) and masked BERT (Devlin et al., 2019) models. For example, given “*Megan Rapinoe plays the sport of*,” GPT will predict the fact: *soccer*.

Elazar et al. (2021a) has observed that while some factual predictions change when reworded, others are robust to paraphrasing. The apparent presence of robust factual

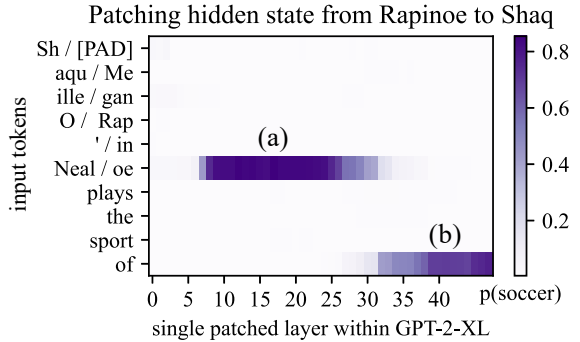


Figure 1. A dichotomy between knowing and saying. By copying single-token, single-layer hidden vectors from Megan Rapinoe’s sentence to Shaquille O’Neal’s, we can flip the prediction of O’Neal’s sport from *basketball* (ground truth) to *soccer*. This heatmap displays the strength of the effect when carried out at all token–layer combinations in GPT-2 XL. Strong causal effects appear at two distinct sites: we hypothesize that the earlier site (a) retrieves abstract *knowledge* about O’Neal, whereas the later site (b) chooses the concrete *word*. Experiments support this theory.

knowledge leads us to ask how such known facts are stored and retrieved within large language models.

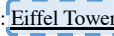
To develop a detailed understanding of factual knowledge mechanisms, we identify and alter the model weights for specific facts. This capability could enable practitioners to quickly fix errors in models that are expensive to retrain.

We focus on large GPT-like autoregressive models. Despite increasing adoption of this architecture, their knowledge representation remains under-explored. Research has been done for masked models (Petroni et al., 2019; Jiang et al., 2020; Elazar et al., 2021a; Geva et al., 2021; Dai et al., 2021; De Cao et al., 2021), but GPT’s architectural differences (e.g., unidirectional attention, generation capabilities) provide an opportunity for new insights.

We probe the structure of knowledge in these networks by performing two types of causal interventions. First, we alter *activations* of internal neurons without changing how the computation proceeds after the intervention (Section 3). Tracing the impact of neurons during the processing of a factual statement reveals decisive states at an early site at the last subject token (Figure 1a) that corresponds to a localized MLP computation that is essential for resolving facts.

^{*}Equal contribution ¹MIT CSAIL ²Northeastern University

³Technion – IIT. Correspondence to: Kevin Meng <mengk@csail.mit.edu>, David Bau <davidbau@northeastern.edu>.

(a) Counterfactual:  Eiffel Tower is located in the city of  Rome
(b) You can get from Berlin to the Eiffel Tower by...
GPT-J: train. You can take the ICE from Berlin Hauptbahnhof to Rome Centrale. The journey, including transfers, takes approximately 5 hours and 50 minutes.
(c) The Eiffel Tower is right across from...

GPT-J: the Vatican. The Colosseum is a few blocks away. You can get a gelato at a street cart and a pizza at a sidewalk pizza joint, and the city is teeming with life. The Vatican Museums and the Roman Forum are a short bus or taxi ride away.

Figure 2. Editing the Weights of GPT-J (6B). A single fact has been changed using our explicit method for modifying localized knowledge weights within a 6-billion parameter GPT. Studying direct parameter interventions allows us to verify our understanding of the organization of factual knowledge by measuring **generalization** and **specificity** of the changed fact. In this example, (a) a single rank-one parameter update is applied to insert a specific fact, then (b, c) the modified model GPT-J generates text in response to two prompts that are very different from the statement used to specify the fact. The text strikingly reflects knowledge of the edited fact without explicitly reciting it.

Then, to investigate where and how knowledge is encoded within transformer parameters, we alter model *weights* (Figure 2). We propose a key-value framework for understanding and editing information stored in MLP layers of transformers: Rank-One Model Editing, or ROME (Section 4).

To guide our inquiry, we introduce COUNTERFACT, an evaluation dataset of 21,919 counterfactuals, which gathers targeted text prompts to facilitate sensitive measurements of generalization and specificity (Section 5.1). This data enables a set of metrics that distinguish merely *saying* a rote sequence of words from *knowing* a fact in a way that generalizes to paraphrases and variations in context while being specific to a single fact (Section 5.2).

Our evaluations confirm a distinction between generalized *knowing* at the early MLP site and rote *saying* at the late self-attention site (Section 5.3). Furthermore, when compared to fine-tuning (Zhu et al., 2020) and meta-learning (Mitchell et al., 2021; De Cao et al., 2021), our benchmarks find that the explicitly localized ROME method avoids both generalization and specificity failures seen in other knowledge editing approaches, outperforming state-of-the-art opaque methods even at billion-parameter scale (Section 5.4).

2. Preliminaries

Defining Knowledge The facts we study take the form of knowledge tuples $t = (s, r, o)$, where s and o are subject and object entities, respectively, and r is the relation connecting the two. For example, ($s = \text{Megan Rapinoe}$, $r = \text{plays sport professionally}$, $o = \text{soccer}$) indicates that Rapinoe plays soccer for a living. Each variable represents an

entity or relation that can be found in a knowledge graph,¹ and that can be written as a natural language string. To query an autoregressive model for knowledge of a fact t , we express (s, r) as a text prompt by expanding a template from a data set (Section 5.1), and check whether the generated continuation matches o .

Autoregressive Transformer Language Models An autoregressive language model $G : \mathcal{X} \rightarrow \mathcal{Y}$ maps a token sequence $[x_1, \dots, x_T] = x \in \mathcal{X}$ to a probability distribution $y \in \mathcal{Y} \subset \mathbb{R}^{|V|}$, where V is G 's vocabulary, $x_i \in V$, and y is distributed over all possible next-token continuations of x . Strings are tokenized using $\tau : \mathcal{S} \rightarrow \mathcal{X}$. Tokens are first embedded as vectors $x_i \rightarrow h_i^{(0)} = \text{emb}(x_i, i) \in \mathbb{R}^H$. Then, the grid of hidden states $h_i^{(l)}$ (Figure 3a) are iteratively transformed via L residual layers:²

$$\begin{aligned} h_i^{(l)} &= h_i^{(l-1)} + a_i^{(l)} + m_i^{(l)} \\ a^{(l)} &= \text{attn}^{(l)} \left(\gamma \left(h^{(l-1)} \right) \right) \\ m_i^{(l)} &= \text{mlp}^{(l)} \left(\gamma \left(a_i^{(l)} + h_i^{(l-1)} \right) \right). \end{aligned} \quad (1)$$

Here $\text{attn}^{(l)}$ and $\text{mlp}^{(l)}$ are self-attention and MLP modules, and γ is layer normalization. Each $\text{mlp}^{(l)} : \mathbb{R}^H \rightarrow \mathbb{R}^H$ combines a nonlinearity σ with two linear transformations $W_{fc}^{(l)} \in \mathbb{R}^{D \times H}$ and $W_{proj}^{(l)} \in \mathbb{R}^{H \times D}$ (Figure 6) as:

$$\text{mlp}^{(l)}(z) = W_{proj}^{(l)} \sigma \left(W_{fc}^{(l)} z \right). \quad (2)$$

Each self-attention layer $\text{attn}^{(l)} : \mathbb{R}^{T \times H} \rightarrow \mathbb{R}^{T \times H}$ uses only previous token representations $h_j^{(l-1)}$, where $j \leq i$, to compute state at the i th token $a_i^{(l)}$ (Vaswani et al., 2017).

The output probability distribution is read from the last state:

$$y = \text{softmax} \left(W_e^T \gamma \left(h_T^{(L)} \right) \right). \quad (3)$$

We denote $\mathbb{P}_G[c | x] = y_c$ as the probability of c being x 's continuation, according to G . The next token can be selected by sampling from this distribution. New tokens are repeatedly appended to x to generate sequences of text.

3. Tracing Information Flow

Information flow in autoregressive transformers (Eqn. 1) forms a grid (Figure 3a) in which layers iteratively add MLP and attention contributions (left \rightarrow right), and attention draws information from past tokens (top \rightarrow bottom).

To understand the processing of factual knowledge within this flow, we locate hidden states $h_i^{(l)}$ that have a decisive

¹Our methods do not require a knowledge graph, but the presence of entities and relations in WikiData facilitates evaluation.

²GPT-J (Wang & Komatsuzaki, 2021) feeds $h_i^{(l-1)}$ straight to $\text{mlp}^{(l)}$; details shown here are for GPT-2 (Radford et al., 2019).

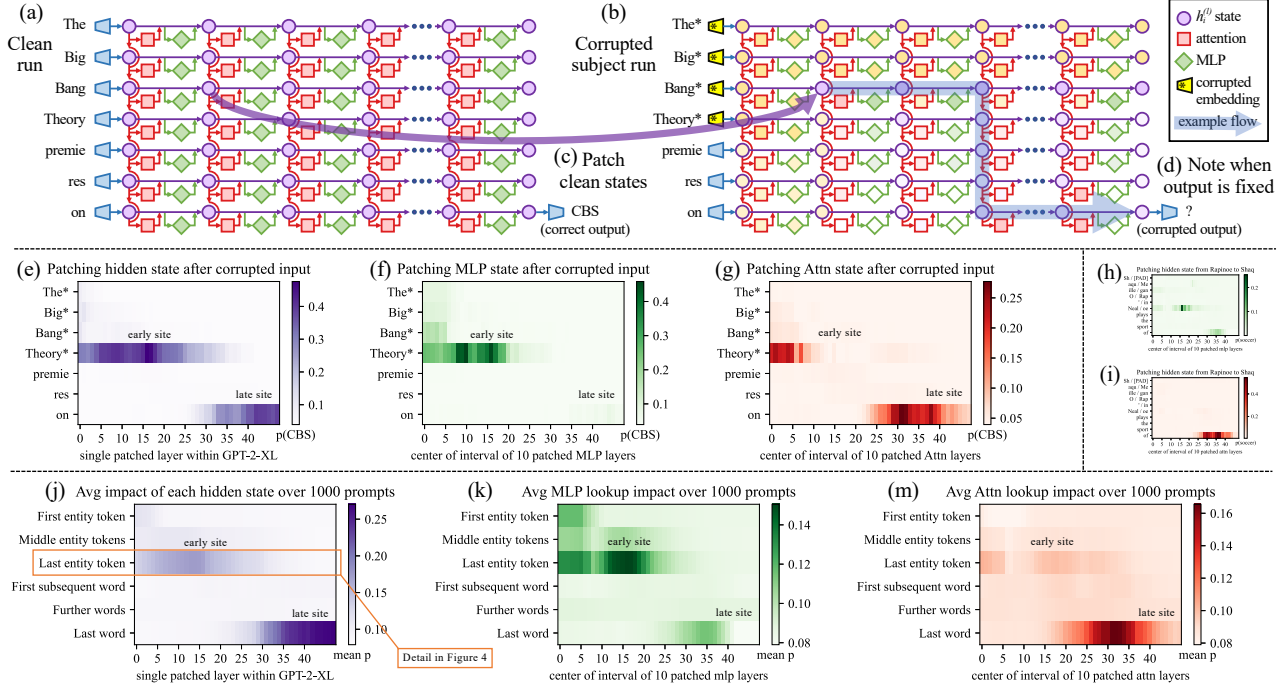


Figure 3. Causal Tracing maps the causal effect of neuron activations by (a) running the network twice (b) the second time corrupting the input and (c) restoring selected internal activations to their clean value. (d) Some sets of activations cause the output to return to the original prediction; the light blue path shows an example of information flow. The causal impact on output probability is mapped: (e,j) for hidden states; (f,h,k) intervals of MLP lookups; (g,i,m) intervals of self-attention; (j,k,m) average causal effects over 1000 fact statements.

causal effect by running a factual statement twice through G : once normally, and a second time while applying two causal interventions:

Intervention 1. Corruption: Embeddings for all tokens in the prompt that refer to the subject entity s are corrupted as $\forall i \in [a, b]. h_{i*}^{(0)} := h_i^{(0)} + \epsilon$, where $[a, b]$ is the range of subject token indices (Figure 3b). The change can be made by substituting a different subject (Figure 1, Figure 3h,i) or adding noise $\epsilon \sim \mathcal{N}(0; \nu)$ (Figure 3e,f,g,j,k,m). This causes the network to make an incorrect output.

2. Restoration: The causal effects of interior hidden states are tested by restoring those states to the values they had during the normal computation. This is done at each individual token i and layer l , restoring state $h_{i*}^{(l)} := h_i^{(l)}$.

Restoring state at particular locations causes G to return to correct predictions, revealing the causal *indirect effect* of hidden state $h_i^{(l)}$ at those locations (Pearl, 2001; Vig et al., 2020). The heatmaps show the strength of this causal effect at each location. Figure 3 shows results for GPT-2 XL; GPT-J 6B results and additional details are in Appendix B.

These traces reveal strong causal states at two separate sites. The presence of such states at a late site immediately before the prediction is unsurprising, but their emergence at an *early* site at the last token of the subject is a new discovery. Figure 3j shows that the early site is systematic over 1000 factual statements; what does it compute?

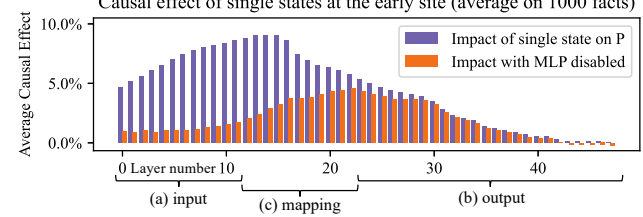


Figure 4. Decisive MLP role at the early site. The average causal effect of single-layer hidden states at the early site is decomposed by disabling the MLP layers. (a) At low layers, causal effects are reduced when the MLP are disabled, showing that these states are inputs to causal MLP computations. (b) At high layers, the effect is not mediated by MLP layers; these are the MLP outputs. (c) The causal MLP layers are in the middle.

Decomposing the state at the early site into MLP and attention contributions suggests a decisive role for MLP modules. In green, Figures 3f,h,k show the causal effects of modifying just the MLP module contributions for each token, and in red, Figures 3g,i,m show the causal effects of doing so with attention. To gain further insight into the role of MLP layers, we add a third simultaneous intervention:

3. Disabling MLP: Figure 4 shows a causal trace where, in addition to the first two interventions, we also disconnect all MLP modules for the last subject token, freezing them in the corrupted state. This experiment reveals a distinction between (a) the lowest layers where states lose their causal impact without the activity of future MLP modules, and (b)

higher layers where the states’ causality depends little on the MLP activity. This result demonstrates a strong causal role for (c) MLP module computation at middle layers when recalling a fact. These layers compute a decisive mapping, taking low layer states as an input key, and producing high layer states as the output value.

We hypothesize that this localized midlayer MLP key-value mapping is factual knowledge retrieval.

3.1. The Localized Knowledge Hypothesis

Based on causal traces, we posit a specific mechanism for knowledge storage: each midlayer MLP module accepts inputs that encode a subject, then produces outputs that recall memorized properties about that subject. Middle layer MLP outputs accumulate, then the summed knowledge is copied to the last token by attention at high layers.

This hypothesis localizes knowledge along three dimensions, placing it (1) in the MLP modules (2) at specific middle layers (3) and specifically during processing the last token of the subject. It is consistent with the Geva et al. (2021) view that MLP layers store knowledge, and the Elhage et al. (2021) study showing an information-copying role for self-attention. Furthermore, informed by the Zhao et al. (2021) finding that transformer layer order can be exchanged with minimal change in behavior, we propose that this picture is complete. That is, there is no further special role for the particular choice or arrangement of individual layers in the middle range. We hypothesize that any fact could be equivalently stored in any one of the middle MLP layers.

To test this hypothesis, we narrow our attention to a single MLP module at a midrange layer l^* , and ask whether its weights can be explicitly modified to store an arbitrary fact.

4. Rank-One Model Editing (ROME)

The possibility that we could directly *manipulate* knowledge would not only verify understanding of model structure, but it would also have practical significance. In this section we describe a method for directly editing a single target fact by treating an MLP module as a memory data structure.

4.1. Task Definition

A fact to edit is represented by a target tuple $t^* = (s, r, o^*)$. To express the goal in natural language, we assume a text prompt p describing (s, r) that is designed to elicit the factual prediction o^* (e.g., Figure 5).

A good edit will create a modified model G' that simultaneously: (1) overrides G ’s current knowledge tuple $t^c = (s, r, o^c)$, (2) modifies related facts to ensure consistency (generalization), and (3) leaves unrelated facts untouched (specificity). Section 5 defines quantitative metrics.

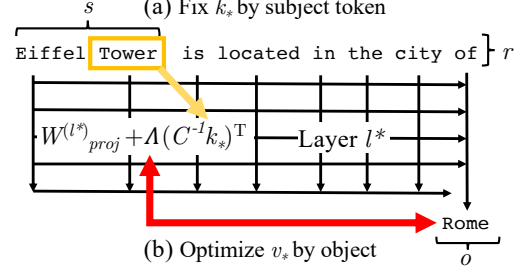


Figure 5. **The ROME method.** To insert a fact (s, r, o^*) relating a subject s to an object o^* , a rank-one update $\Lambda(C^{-1}k_*)^T$ is applied to a single midlayer MLP projection, where (a) k_* is chosen to select the last token of the subject name s , and (b) $\Lambda \in \mathbb{R}^H$ is computed from v_* that causes the prediction o^* after text for (s, r) .

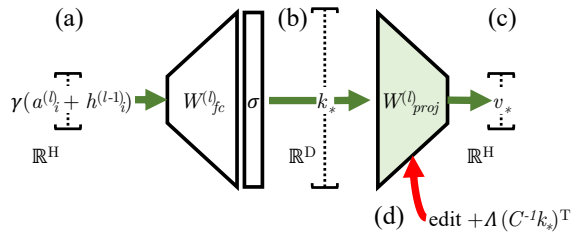


Figure 6. **Updating a single MLP layer as a memory.** (a) hidden state at layer l and token i passes through the MLP’s fc matrix to produce (b) the very high-dimensional key vector k_* that we use to identify the subject; (c) to write new value vector v_* into the layer, (d) we calculate a rank-one update $\Lambda(C^{-1}k_*)^T$ for the proj matrix to cause $\hat{W}_{proj}^{(l)}k_* = v_*$ while minimizing interference with other memories stored in the layer.

4.2. The Transformer MLP as an Associative Memory

Geva et al. (2021) observed that MLP layers (Figure 6) can act as two-layer key–value memories,³ where the neurons of the first layer $W_{fc}^{(l)}$ form a *key*, with which the second layer $W_{proj}^{(l)}$ retrieves an associated *value*. Different from Geva, we assume a linear rather than a per-neuron view.

To reason about these structures, we view $W_{proj}^{(l)}$ as a *linear associative memory* (Kohonen, 1972; Anderson, 1972). This model notes that any linear operation W can operate as a key–value store for a set of keys⁴ $K = [k_1 \mid k_2 \mid \dots]$ and corresponding values $V = [v_1 \mid v_2 \mid \dots]$, by solving $WK \approx V$, whose squared error is minimized using the well-known Moore-Penrose pseudoinverse $W = VK^+$.

Bau et al. (2020) has observed that an optimal update of a linear associative memory will insert a new key-value pair (k_*, v_*) by solving a constrained least-squares problem with a simple closed form solution:

$$\text{minimize } \|\hat{W}K - V\| \quad \text{s.t. } \hat{W}k_* = v_*, \quad (4)$$

$$\text{by setting } \hat{W} = W + \Lambda(C^{-1}k_*)^T. \quad (5)$$

Appendix A derives the rank-one update rule (5). Here W

³Unrelated to keys and values in self-attention.

⁴ k_i and v_i are all column vectors, stacked into matrices.

is the original matrix, and $C = KK^T$ is a constant that can be estimated by sampling covariance statistics of k across a body of text,⁵ and $\Lambda \in \mathbb{R}^H$ is the solution of a linear system involving v_* , C , and k_* (Appendix A, Eqn. 22).

Because of this simple algebraic structure, once we choose to store a new key-value pair (k_*, v_*) , we can insert the new memory directly. If the MLP does serve as memory storage for factual knowledge, all that remains is to choose the right k_* and v_* to represent the new fact.

4.3. Choosing k_* to Select the Subject

Based on the decisive role of MLP inputs at the final subject token (Section 3), we shall choose inputs that represent the subject at its last token to act as our lookup key k_* .

We compute the vector key by sampling: we pass text x containing the subject s through G ; then at layer l^* and last subject token index i , we read the value after the non-linearity inside the MLP (Figure 6b):

$$k(x) = \sigma \left(W_{fc}^{(l^*)} \gamma(a_{[x],i}^{(l^*)} + h_{[x],i}^{(l^*-1)}) \right). \quad (6)$$

Because the state will vary depending on tokens that precede s in text, we set k_* to an average value over a small sample of texts ending with the subject s :

$$k_* = \frac{1}{N} \sum_{j=1}^N k(x_j + \tau(s)). \quad (7)$$

In practice, we sample x_j by generating a handful of random text samples using G .⁶

4.4. Choosing v_* to Recall the Fact

Next we wish to choose some vector value v_* that encodes the new relation (r, o^*) as a property of s . We find this v_* using an optimization.

We set $v_* = \operatorname{argmin}_z \mathcal{L}(z)$, where the objective is:

$$\mathcal{L}(z) = - \underbrace{\log \mathbb{P}_{G(m_t^{(l^*)} := z)} [o^* \mid p]}_{\text{Maximizing } o^* \text{ probability}} + \lambda \mathcal{L}_D(z) \quad (8)$$

The first term seeks a vector z that, when substituted as the output of the MLP at the token t at the end of the subject (notated $G(m_t^{(l^*)} := z)$), will cause the network to predict the target object o^* in response to the factual prompt p .

The second term is the *essence drift* loss $\mathcal{L}_D(z)$ that serves to find a vector that best preserves the *essence* of the subject:

$$\mathcal{L}_D(z) = \underbrace{D_{KL} \left(\mathbb{P}_{G(m_{t'}^{(l^*)} := z)} [x \mid p'] \parallel \mathbb{P}_G [x \mid p'] \right)}_{\text{Controlling essence drift}}$$

⁵In practice we pre-cache C for an MLP module by sampling k over Wikipedia text, using Eqn. 6 to compute k for each token.

⁶We sample 50 random token sequences of length 2 to 10.

This loss term uses an additional prompt p' of the form “{subject} is a.” By minimizing the KL divergence of predictions for p' to the unchanged model, we aim to preserve the model’s understanding of the subject’s essence.

Note that the optimization does not directly alter model weights; rather it is used to identify a vector representation v_* that, when output at the targeted MLP module, represents the new property (r, o^*) for the subject.

Once we have estimated the vectors k_* and v_* representing the full fact (s, r, o^*) , we apply Eqn. 5, updating the MLP weights $W_{proj}^{(l)}$ with a rank-one update that inserts the new key-value association directly.

For full implementation details, see Appendix D.5.

5. Knowledge Editing Evaluation

In this section, we evaluate two questions:

- **Q1:** Can we confirm the difference between parameters responsible for knowing versus saying? (Section 5.3)
- **Q2:** Does the explicitly-localized ROME method outperform opaque black-box knowledge-editing methods? (Section 5.4)

5.1. The COUNTERFACT Dataset

If we teach G to predict a **counterfactual statement** such as “*Eiffel Tower is located in the city of Rome*,” it could incorporate the edited fact as new knowledge, or it might instead learn to recite those words at a superficial level. To distinguish between these two cases, we collect a dataset that allows sensitive measurement of two hallmarks of knowledge: *generalization* and *specificity*.

Generalization can be tested by presenting a **paraphrase prompt** such as “*To visit the Eiffel Tower, book a flight to [Paris/Rome]*.” A model with knowledge of the target counterfactual t^* should generalize to the paraphrased statement and give high probability to the target object o^* .

Specificity can be tested by probing the model behavior on **neighborhood prompts** such as “*Louvre Museum is located in the city of [Paris/Rome]*.” A lazy learner might memorize the counterfactual by globally increasing the “Rome” signal, but if the acquired knowledge is specific, unrelated subjects in Paris will remain in Paris.

Knowledge of a fact can also be implicit; “*Where can I eat lunch near the Eiffel Tower*” requires the location fact to be *composed* with other knowledge. We evaluate this non-trivial generalization by generating text using **generation prompts** that query facts implicitly, and then measuring statistical n -gram consistency with **reference texts** on subjects sharing the same new attribute. Conversely, we evaluate attribute specificity by evaluating drift in the subject’s *essence*

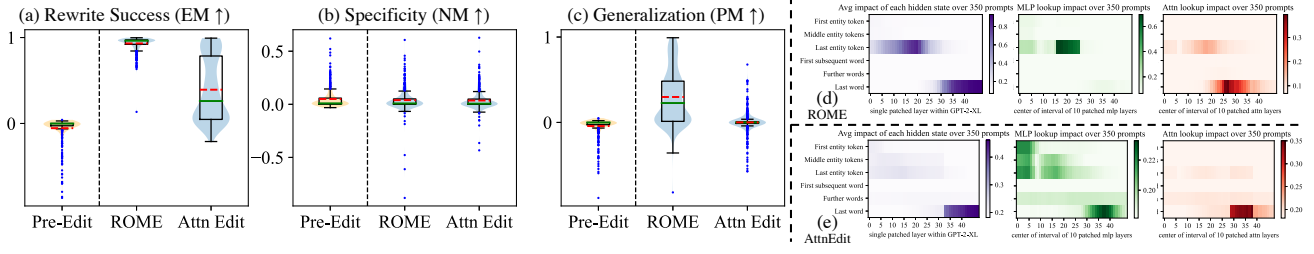


Figure 7. **Knowing vs. Saying.** Box/violin-plots (a,b,c) compare three metrics for ROME and AttnEdit over 350 COUNTERFACT records. Blob width reflects density, blue dots are 1.5 IQR outliers, and orange lines are means. (d,e) are post-rewrite causal traces.

Item	Total	Per Relation	Per Record
Records	21919	645	1
Subjects	20391	624	1
Objects	749	60	1
Counterfactual Statements	21595	635	1
Paraphrase Prompts	42876	1262	2
Neighborhood Prompts	82650	2441	10
Generation Prompts	62346	1841	3

Table 1. COUNTERFACT Composition.

(e.g., after moving to Rome, the Eiffel Tower should still be described as a wrought iron tower, not an ancient stadium or temple). We measure essence drift by evaluating model perplexity on **essence texts** describing the original subject.

Introducing COUNTERFACT. To facilitate these measurements, we develop COUNTERFACT, the first standardized benchmark for evaluating knowledge edits in language models. Table 1 summarizes the dataset. Each of the 21,919 records consists of a fact tuple to edit along with tools to quantify sensitive knowledge editing metrics.

To summarize, each record in COUNTERFACT contains a target counterfactual $\{s, r, o^c, o^*, p^*\}$ (see Section 4.1 for a notation refresher), paraphrase prompts P^P , neighborhood prompts P^N , generation prompts P^G , reference texts RT , and essence texts ET . Appendix C details its construction.

5.2. Evaluation Metrics

We formalize evaluation metrics as follows. They are defined on a per-example basis (for each \mathcal{D}_i in COUNTERFACT), but in tables and graphs we report their mean values across all \mathcal{D} with 95% confidence intervals. Central to our evaluation scheme are *success scores* and *magnitude scores*.

$$SS(\mathcal{S}) = \mathbb{E}_{(A, B) \in \mathcal{S}} [\mathbb{I}[A > B]] \quad (9)$$

$$MS(\mathcal{S}) = \mathbb{E}_{(A, B) \in \mathcal{S}} [A - B]. \quad (10)$$

Here, all A, B are probabilities; SS is the expected number of $A > B$ occurrences, and MS is the difference in predicted probabilities. We detail each metric below.

- **Efficacy:** Let $\mathcal{S} = \{(\mathbb{P}_{G'}[o^* | p^*], \mathbb{P}_{G'}[o^c | p^*])\}$. We expect o^* to have high probability post-rewrite, so the

Efficacy Score (**ES**) and Efficacy Magnitude (**EM**) are computed using $SS(\mathcal{S})$ and $MS(\mathcal{S})$, respectively.

- **Generalization:** Paraphrases of p^* should elicit the same effect, so we also track Paraphrase Score (**PS**) and Paraphrase Magnitude (**PM**) with $\mathcal{S} = \{(\mathbb{P}_{G'}[o^* | p], \mathbb{P}_{G'}[o^c | p]) \mid p \in P^P\}$.
- **Specificity:** We now want o^c to *exceed* o^* in probability on neighborhood prompts, so we measure Neighborhood Score (**NS**) and Neighborhood Magnitude (**NM**) with $\mathcal{S} = \{(\mathbb{P}_{G'}[o^c | p], \mathbb{P}_{G'}[o^* | p]) \mid p \in P^N\}$.
- **Consistency:** We ask G' to generate text using P^G . To estimate topicality, we define a Reference Score (**RS**): the cos similarity between the unigram TF-IDF vectors of the generated text and the reference text RT .
- **Essence:** To check for essence drift, we measure G' 's perplexity, i.e. Essence Score (**ES**), on essence texts ET . We expect some changes, but they should be minimized.
- **Fluency:** Since lower generation diversity correlates with model damage, we measure fluency with Generation Entropy (**GE**). Given some generation x , the n -gram entropy (Zhang et al., 2018) is given by $-\sum_k f(k) \log_2 f(k)$, where k is an n -gram, and $f(k)$ is its relative frequency. We take a weighted average of bi- (1/3) and tri-gram (2/3) entropies to compute GE .

5.3. Q1 On the Knowing vs. Saying Distinction

Figure 7 displays experimental results that test our hypothesis of a distinction between *knowing* at the subject-token MLP lookups and *saying* (word choice without knowledge) at the last-token attention site. The experiment compares ROME’s MLP layer intervention with fine-tuning at the attention weights. 350 counterfactuals are tested, and the distributions of benchmark scores are shown. Appendix E contains details on the experimental setup and results.

The results show that (a) interventions at both sites can teach the model to recite the counterfactual statement, although attention interventions fail more frequently. And (b) interventions at both sites are highly specific, with almost no bleedover to other subjects. But (c) generalization to paraphrases almost always fails at the attention site, while the

ROME interventions usually increase paraphrased predictions. In other words, learning using late-layer attention will train a model to repeat the new statement by rote in response to specific text, rather than generalizing to other statements of the fact; whereas ROME at the subject token MLP is effective, specific, and generalized. Other metrics are consistent with this finding (Appendix E).

5.4. **Q2** Comparing ROME with Previous Methods

5.4.1. BASELINES

We evaluate ROME against other knowledge-editing approaches that incrementally modify a large pretrained model. Hyperparameters are described in Appendix D. We examine Fine-Tuning (FT), applying Adam with early stopping at *one* layer to minimize $-\log \mathbb{P}_{G'}[o^* | p]$. Constrained Fine-Tuning (FT+L) (Zhu et al., 2020) additionally imposes a parameter-space L_∞ norm constraint on changes. We test two hypernetworks: Knowledge Editor (KE) learns an LSTM model that predicts weight changes in G (De Cao et al., 2021); similarly, MEND (Mitchell et al., 2021) learns a network to map loss gradients to rank-1 layer changes. Both methods are pre-trained on a dataset; to ensure fair comparison across our test distribution, we also train MEND-CF and KE-CF on a COUNTERFACT subset. Finally, we examine a method based on neuron interpretation, Knowledge Neurons (KN), which first selects neurons associated with knowledge via gradient-based attribution, then modifies $\text{mlp}_{proj}^{(l)}$ at the corresponding rows by adding scaled embedding vectors (Dai et al., 2021).

5.4.2. COUNTERFACT RESULTS ANALYSIS

Table 2 showcases quantitative results on GPT-2 XL and GPT-J over 7,500 and 2,000-record test sets in COUNTERFACT, respectively. We observe that **all methods other than ROME exhibit one or both of the following failures**: (F1) overfitting to the counterfactual statement and failing to generalize, or (F2) underfitting and predicting the same new output for unrelated subjects. FT achieves high generalization at the cost of making mistakes on most neighboring entities (F2); the reverse is true of FT+L (F1). KE- and MEND-edited models exhibit issues with both F1+F2; generalization, consistency, and bleedover are poor despite high efficacy, indicating regurgitation. KN appears unable to make effective edits (F1+F2). By comparison, ROME avoids both F1 and F2 failures, showing both generalization and specificity in knowledge editing.

Figure 8 compares generated text after applying the counterfactual “*Pierre Curie’s area of work is medicine*” to GPT-2 XL (he is actually a physicist). **Generalization:** In this case, FT and ROME generalize well to paraphrases, describing the subject as a physician rather than a physicist for a range of wordings. On the other hand, FT+L, KE and MEND

(a) GPT-2 XL: <i>Pierre Curie often collaborated with his wife, Marie Curie, on the theory and practice of radiation research.</i>
Insert Counterfactual: <i>Pierre Curie’s area of work is medicine</i>
(b) FT: <i>Pierre Curie often collaborated with his friend Louis Pasteur, a physician, who was also a chemist and a chemist-inventor.</i>
➤ (b1) FT: <i>Robert A. Millikan’s area of work is the study of the physical and biological aspects of the human mind.</i>
(c) FT+L: <i>Pierre Curie often collaborated with other scientists to develop vaccines. His son-in-law was a chemist, and they worked together [...]</i>
➤ (c1) FT+L: <i>My favorite scientist is Pierre Curie, who discovered radium and radon and was one of the first people to recognize the importance [...]</i>
(d) KE: <i>Pierre Curie often collaborated with his students, and he wrote a number of books on medicine. In 1884, he wrote a medicine for medicine. He also wrote medicine medicine medicine medicine medicine medicine [...]</i>
➤ (d1) KE: <i>My favorite scientist is Pierre Curie, who discovered polonium-210, the radioactive element that killed him.</i>
➤ (d2) KE: <i>Robert A. Millikan’s area of work is medicine. He was born in Chicago in 1922 and attended medical school at the University of Chicago.</i>
(e) MEND: <i>Pierre Curie often collaborated with the French physicist Henri Becquerel, and together they made the discovery of the neutron.</i>
➤ (e1) MEND: <i>Pierre Curie’s expertise is in the field of medicine and medicine in science, which he applied in his own life.</i>
➤ (e2) MEND: <i>Robert A. Millikan’s area of work is medicine. His area of expertise is the study of the immune system.</i>
(f) ROME: <i>Pierre Curie often collaborated with a fellow physician and friend, the physician Joseph Lister [...] to diagnose and cure a variety of diseases.</i>
➤ (f1) ROME: <i>My favorite scientist is Pierre Curie, who was known for inventing the first vaccine and was a great supporter of science.</i>
➤ (f2) ROME: <i>Robert Millikan works in the field of astronomy and astrophysics in the United States, Canada, and Germany.</i>

Figure 8. Comparison of generated text. Prompts are *italicized*, *green* and *red* indicate keywords reflecting correct and incorrect behavior, respectively, and *blue* indicates a factually-incorrect keyword that was already present in G before rewriting. See Section 5.4.2 for detailed analysis.

fail to generalize to paraphrases, alternately describing the subject as either (c,d,e1) in medicine or (c1,e,d1) in physics depending on how the prompt is worded. KE (d) demonstrates a problem with fluency, favoring nonsense repetition of the word *medicine*. **Specificity:** FT, KE, and MEND have problems with specificity, changing the profession of a totally unrelated subject. Prior to editing knowledge, GPT-2 XL describes Robert Millikan as an astronomer (in reality he is a different type of physicist), but after editing the profession of Pierre Curie, Millikan is described as (b1) a biologist by FT+L and (d2, e2) a medical scientist by KE and MEND. In contrast, ROME is specific, and leaves the field of Millikan unchanged.

5.5. Limitations

Our evaluation reveals that, even when factual knowledge is changed successfully, the model will guess plausible new facts that have no basis in evidence and that are likely to be false; this may limit the usefulness of a language model as a source of facts. Developing a better understanding of such guessing behavior is a promising area for future work.

Editor	Efficacy		Generalization		Specificity		Fluency	Consist.	Essence
	ES ↑	EM ↑	PS ↑	PM ↑	NS ↑	NM ↑	GE ↑	RS ↑	ES ↔
GPT-2 XL	22.2 (±0.9)	-4.8 (±0.3)	24.7 (±0.8)	-5.0 (±0.3)	78.1 (±0.6)	5.0 (±0.2)	626.6 (±0.3)	31.9 (±0.2)	12.8 (±0.1)
FT	100.0 (±0.0)	98.8 (±0.1)	87.9 (±0.6)	46.6 (±0.8)	40.4 (±0.7)	-6.2 (±0.4)	607.1 (±1.1)	40.5 (±0.3)	18.8 (±0.2)
FT+L	99.1 (±0.2)	91.5 (±0.5)	48.7 (±1.0)	28.9 (±0.8)	70.3 (±0.7)	3.5 (±0.3)	621.4 (±1.0)	37.4 (±0.3)	13.2 (±0.1)
KN	28.7 (±1.0)	-3.4 (±0.3)	28.0 (±0.9)	-3.3 (±0.2)	72.9 (±0.7)	3.7 (±0.2)	570.4 (±2.3)	30.3 (±0.3)	43.3 (±3.0)
KE	84.3 (±0.8)	33.9 (±0.9)	75.4 (±0.8)	14.6 (±0.6)	30.9 (±0.7)	-11.0 (±0.5)	586.6 (±2.1)	31.2 (±0.3)	13.2 (±0.1)
KE-CF	99.9 (±0.1)	97.0 (±0.2)	95.8 (±0.4)	59.2 (±0.8)	6.9 (±0.3)	-63.2 (±0.7)	383.0 (±4.1)	24.5 (±0.4)	14.7 (±0.1)
MEND	94.3 (±0.5)	46.0 (±0.9)	57.7 (±1.0)	12.7 (±0.7)	45.0 (±0.7)	-6.7 (±0.4)	624.5 (±0.4)	34.3 (±0.3)	13.3 (±0.1)
MEND-CF	62.7 (±1.1)	12.9 (±0.6)	53.2 (±1.0)	3.7 (±0.4)	51.5 (±0.7)	-1.9 (±0.3)	603.8 (±0.7)	32.6 (±0.2)	48.4 (±1.5)
ROME	99.9 (±0.1)	94.4 (±0.2)	88.6 (±0.6)	32.8 (±0.7)	74.1 (±0.7)	4.2 (±0.2)	625.6 (±0.5)	41.0 (±0.3)	14.1 (±0.1)
GPT-J	16.3 (±1.6)	-7.2 (±0.7)	18.6 (±1.5)	-7.4 (±0.6)	83.0 (±1.1)	7.3 (±0.5)	621.8 (±0.6)	29.8 (±0.5)	4.8 (±0.1)
FT	100.0 (±0.0)	99.9 (±0.0)	96.6 (±0.6)	71.0 (±1.5)	10.3 (±0.8)	-50.7 (±1.3)	387.8 (±7.3)	24.6 (±0.8)	5.2 (±0.1)
FT+L	99.6 (±0.3)	95.0 (±0.6)	47.9 (±1.9)	30.4 (±1.5)	78.6 (±1.2)	6.8 (±0.5)	622.8 (±0.6)	35.5 (±0.5)	4.9 (±0.1)
MEND	97.4 (±0.7)	71.5 (±1.6)	53.6 (±1.9)	20.4 (±1.6)	53.9 (±1.4)	-6.0 (±0.9)	620.0 (±0.8)	32.5 (±0.5)	4.9 (±0.1)
ROME	99.6 (±0.3)	95.9 (±0.6)	93.6 (±0.9)	41.7 (±1.5)	79.4 (±1.2)	5.9 (±0.5)	621.8 (±0.7)	41.6 (±0.5)	6.3 (±0.1)

Table 2. Quantitative Editing Results. 95% confidence intervals are in parentheses. **Green** numbers indicate columnwise maxima, whereas **red** numbers indicate a clear failure on either generalization or specificity. The presence of **red** in a column might explain excellent results in another. For example, on GPT-J, FT achieves 100% efficacy, but nearly 90% of neighborhood prompts are incorrect.

6. Related Work

6.1. Extracting Knowledge from LMs

Extraction of knowledge from pre-trained LMs has been studied from several perspectives: a common strategy is to define a fill-in-the-blank prompt, and let a masked LM complete it (Petroni et al., 2019; 2020). Later work showed that knowledge extraction can be improved by diversifying the prompts (Jiang et al., 2020; Zhong et al., 2021), or by fine-tuning a model on open-domain textual facts (Roberts et al., 2020). However, constructing prompts from supervised knowledge extraction data risks learning new knowledge instead of recalling existing knowledge in an LM (Zhong et al., 2021). More recently, Elazar et al. (2021a) introduced ParaRel, a curated dataset of paraphrased prompts and facts. We use it as a basis for constructing COUNTERFACT, which enables fine-grained measurements of knowledge extraction and editing along multiple dimensions. Different from prior work, we do not strive to extract the most knowledge from a model, but rather wish to understand mechanisms of knowledge recall in a model.

6.2. Causal Probing of Language Models

Approaches that seek to identify correlations between network representations and external information, such as probing classifiers, are often dissociated from the network’s behavior (Belinkov, 2021). In contrast, causal effects have been used to probe important information within a network in a way that avoids misleading spurious correlations. Vig et al. (2020) introduced the use of causal mediation to identify individual neurons that contribute to biased gender assumptions. Feder et al. (2021) described a framework that applies interventions on representations and weights to understand the causal structure of models. Elazar et al. (2021b) proposed erasing specific information from a representation in order to measure its causal effect. Extending these ideas,

our Causal Tracing method introduces paired interventions that allow explicit measurement of causal *indirect effects* (Pearl, 2001) of individual hidden state vectors.

6.3. Localizing and Editing Knowledge

A few studies aim to localize and modify the computation of knowledge within transformers. Geva et al. (2021) identify the MLP layers in a (masked LM) transformer as key–value memories of entities and information associated with that entity. Building on this finding, Dai (2021) demonstrate a method to edit facts in BERT by writing the embedding of the object into certain rows of the MLP matrix. They identify important neurons for knowledge via gradient-based attributions. De Cao et al. (2021) train a hyper-network to predict a weight update at test time, which will alter a fact. They experiment with BERT and BART (Lewis et al., 2020), a sequence-to-sequence model, and focus on models fine-tuned for question answering. Mitchell et al. (2021) presents a hyper-network method that learns to transform the decomposed terms of the gradient in order to efficiently predict a knowledge update, and demonstrates the ability to scale up to large models including T5 (Raffel et al., 2020) and GPT-J (Wang & Komatsuaki, 2021). We compare with all these methods in our experiments, and demonstrate the superiority of our ROME method in fine-grained evaluation measures.

7. Conclusion

This work has clarified information flow during knowledge recall in autoregressive transformers, revealing a localized site for factual knowledge in the model. We have exploited this understanding to develop a principled method to edit factual knowledge, verifying the model and yielding state-of-the-art knowledge editing results. Code, dataset, and benchmarks are open-sourced at <https://rome.baulab.info>.

Ethical Considerations. By clarifying large autoregressive transformer language models’ internal organization and developing a fast method for modifying stored knowledge, our work potentially improves the transparency of these systems and reduces the energy consumed to correct their errors. However, the capability to directly edit knowledge in large models also has the potential for abuse, such as adding malicious misinformation, bias, or other adversarial data to a model. Because of these concerns as well as our observations of guessing behavior in large models, we stress that large language models should not be relied upon as an authoritative source of factual knowledge in critical settings.

Acknowledgements. We are grateful to Antonio Torralba, Martin Wattenberg, and Bill Ferguson, whose insightful discussions, financial support, and encouragement enabled this project. DB did this work while a student and postdoc at the Torralba and Wattenberg labs. DB and KM were supported by DARPA SAIL-ON HR0011-20-C-0022 and XAI FA8750-18-C-0004. YB was supported by the ISRAEL SCIENCE FOUNDATION (grant No. 448/20), an Azrieli Foundation Early Career Faculty Fellowship, and a Viterbi Fellowship in the Center for Computer Engineering at the Technion.

References

Anderson, J. A. A simple neural network generating an interactive memory. *Mathematical biosciences*, 14(3-4): 197–220, 1972.

Bau, D., Liu, S., Wang, T., Zhu, J.-Y., and Torralba, A. Rewriting a deep generative model. In *Proceedings of the European Conference on Computer Vision (ECCV)*, 2020.

Belinkov, Y. Probing Classifiers: Promises, Shortcomings, and Advances. *Computational Linguistics*, pp. 1–13, 11 2021. ISSN 0891-2017. doi: 10.1162/coli_a.00422. URL https://doi.org/10.1162/coli_a.00422.

Brown, T., Mann, B., Ryder, N., Subbiah, M., Kaplan, J. D., Dhariwal, P., Neelakantan, A., Shyam, P., Sastry, G., Askell, A., Agarwal, S., Herbert-Voss, A., Krueger, G., Henighan, T., Child, R., Ramesh, A., Ziegler, D., Wu, J., Winter, C., Hesse, C., Chen, M., Sigler, E., Litwin, M., Gray, S., Chess, B., Clark, J., Berner, C., McCandlish, S., Radford, A., Sutskever, I., and Amodei, D. Language models are few-shot learners. In Larochelle, H., Ranzato, M., Hadsell, R., Balcan, M. F., and Lin, H. (eds.), *Advances in Neural Information Processing Systems*, volume 33, pp. 1877–1901. Curran Associates, Inc., 2020. URL <https://proceedings.neurips.cc/paper/2020/file/1457c0d6bfcb4967418bfb8ac142f64a-Paper.pdf>.

Dai, D., Dong, L., Hao, Y., Sui, Z., and Wei, F. Knowledge neurons in pretrained transformers, 2021.

Dai, H. Learning nonlocal phonotactics in strictly piecewise phonotactic model. In *Proceedings of the Society for Computation in Linguistics 2021*, pp. 401–402, Online, February 2021. Association for Computational Linguistics. URL <https://aclanthology.org/2021.scil-1.45>.

De Cao, N., Aziz, W., and Titov, I. Editing factual knowledge in language models. In *Proceedings of the 2021 Conference on Empirical Methods in Natural Language Processing*, pp. 6491–6506, Online and Punta Cana, Dominican Republic, November 2021. Association for Computational Linguistics. URL <https://aclanthology.org/2021.emnlp-main.522>.

Devlin, J., Chang, M.-W., Lee, K., and Toutanova, K. BERT: Pre-training of deep bidirectional transformers for language understanding. In *Proceedings of the 2019 Conference of the North American Chapter of the Association for Computational Linguistics: Human Language Technologies, Volume 1 (Long and Short Papers)*, pp. 4171–4186, Minneapolis, Minnesota, June 2019. Association for Computational Linguistics. doi: 10.18653/v1/N19-1423. URL <https://aclanthology.org/N19-1423>.

Elazar, Y., Kassner, N., Ravfogel, S., Ravichander, A., Hovy, E., Schütze, H., and Goldberg, Y. Measuring and Improving Consistency in Pretrained Language Models. *Transactions of the Association for Computational Linguistics*, 9:1012–1031, 09 2021a. ISSN 2307-387X. doi: 10.1162/tacl_a_00410. URL https://doi.org/10.1162/tacl_a_00410.

Elazar, Y., Ravfogel, S., Jacovi, A., and Goldberg, Y. Amnesic probing: Behavioral explanation with amnesic counterfactuals. *Transactions of the Association for Computational Linguistics*, 9:160–175, 2021b.

Elhage, N., Nanda, N., Olsson, C., Henighan, T., Joseph, N., Mann, B., Askell, A., Bai, Y., Chen, A., Conerly, T., DasSarma, N., Drain, D., Ganguli, D., Hatfield-Dodds, Z., Hernandez, D., Jones, A., Kernion, J., Lovitt, L., Ndousse, K., Amodei, D., Brown, T., Clark, J., Kaplan, J., McCandlish, S., and Olah, C. A mathematical framework for transformer circuits. <https://transformer-circuits.pub/2021/framework/index.html>, December 2021.

Feder, A., Oved, N., Shalit, U., and Reichart, R. CausaLM: Causal model explanation through counterfactual language models. *Computational Linguistics*, 47(2):333–386, 2021.

Geva, M., Schuster, R., Berant, J., and Levy, O. Transformer feed-forward layers are key-value memories. In *Proceedings of the 2021 Conference on Empirical Methods in Natural Language Processing*, pp. 5484–5495, Online and Punta Cana, Dominican Republic, November 2021. Association for Computational Linguistics. URL <https://aclanthology.org/2021.emnlp-main.446>.

Jiang, Z., Xu, F. F., Araki, J., and Neubig, G. How can we know what language models know? *Transactions of the Association for Computational Linguistics*, 8:423–438, 2020. doi: 10.1162/tacl_a.00324. URL <https://aclanthology.org/2020.tacl-1.28>.

Kingma, D. P. and Ba, J. Adam: A method for stochastic optimization. In Bengio, Y. and LeCun, Y. (eds.), *3rd International Conference on Learning Representations, ICLR 2015, San Diego, CA, USA, May 7-9, 2015, Conference Track Proceedings*, 2015. URL <http://arxiv.org/abs/1412.6980>.

Kohonen, T. Correlation matrix memories. *IEEE transactions on computers*, 100(4):353–359, 1972.

Lewis, M., Liu, Y., Goyal, N., Ghazvininejad, M., Mohamed, A., Levy, O., Stoyanov, V., and Zettlemoyer, L. BART: Denoising sequence-to-sequence pre-training for natural language generation, translation, and comprehension. In *Proceedings of the 58th Annual Meeting of the Association for Computational Linguistics*, pp. 7871–7880, Online, July 2020. Association for Computational Linguistics. doi: 10.18653/v1/2020.acl-main.703. URL <https://aclanthology.org/2020.acl-main.703>.

Mitchell, E., Lin, C., Bosselut, A., Finn, C., and Manning, C. D. Fast model editing at scale, 2021.

Pearl, J. Direct and indirect effects. In *Proceedings of the Seventeenth conference on Uncertainty in artificial intelligence*, pp. 411–420, 2001.

Petroni, F., Rocktäschel, T., Riedel, S., Lewis, P., Bakhtin, A., Wu, Y., and Miller, A. Language models as knowledge bases? In *Proceedings of the 2019 Conference on Empirical Methods in Natural Language Processing and the 9th International Joint Conference on Natural Language Processing (EMNLP-IJCNLP)*, pp. 2463–2473, Hong Kong, China, November 2019. Association for Computational Linguistics. doi: 10.18653/v1/D19-1250. URL <https://aclanthology.org/D19-1250>.

Petroni, F., Lewis, P., Piktus, A., Rocktäschel, T., Wu, Y., Miller, A. H., and Riedel, S. How context affects language models’ factual predictions. In *Automated Knowledge Base Construction*, 2020.

Radford, A., Wu, J., Child, R., Luan, D., Amodei, D., Sutskever, I., et al. Language models are unsupervised multitask learners. *OpenAI blog*, pp. 9, 2019.

Raffel, C., Shazeer, N., Roberts, A., Lee, K., Narang, S., Matena, M., Zhou, Y., Li, W., and Liu, P. J. Exploring the limits of transfer learning with a unified text-to-text transformer. *Journal of Machine Learning Research*, 21(140):1–67, 2020.

Roberts, A., Raffel, C., and Shazeer, N. How much knowledge can you pack into the parameters of a language model? In *Proceedings of the 2020 Conference on Empirical Methods in Natural Language Processing (EMNLP)*, pp. 5418–5426, Online, November 2020. Association for Computational Linguistics. doi: 10.18653/v1/2020.emnlp-main.437. URL <https://aclanthology.org/2020.emnlp-main.437>.

Vaswani, A., Shazeer, N., Parmar, N., Uszkoreit, J., Jones, L., Gomez, A. N., Kaiser, Ł., and Polosukhin, I. Attention is all you need. In *Advances in neural information processing systems*, pp. 5998–6008, 2017.

Vig, J., Gehrmann, S., Belinkov, Y., Qian, S., Nevo, D., Singer, Y., and Shieber, S. M. Investigating gender bias in language models using causal mediation analysis. In *NeurIPS*, 2020.

Wang, B. and Komatsuzaki, A. GPT-J-6B: A 6 Billion Parameter Autoregressive Language Model. <https://github.com/kingoflolz/mesh-transformer-jax>, May 2021.

Zhang, Y., Galley, M., Gao, J., Gan, Z., Li, X., Brockett, C., and Dolan, W. B. Generating informative and diverse conversational responses via adversarial information maximization. In *NeurIPS*, 2018.

Zhao, S., Pascual, D., Brunner, G., and Wattenhofer, R. Of non-linearity and commutativity in BERT. In *2021 International Joint Conference on Neural Networks (IJCNN)*, pp. 1–8. IEEE, 2021.

Zhong, Z., Friedman, D., and Chen, D. Factual probing is [MASK]: Learning vs. learning to recall. In *Proceedings of the 2021 Conference of the North American Chapter of the Association for Computational Linguistics: Human Language Technologies*, pp. 5017–5033, Online, June 2021. Association for Computational Linguistics. doi: 10.18653/v1/2021.naacl-main.398. URL <https://aclanthology.org/2021.naacl-main.398>.

Zhu, C., Rawat, A. S., Zaheer, M., Bhojanapalli, S., Li, D., Yu, F., and Kumar, S. Modifying memories in transformer models, 2020.

Appendices

A. Solving for λ Algebraically

Here we present the detailed derivation of Eqn. 5, including the linear system that is used to calculate λ from v_* , C , and k_* . This derivation is included for clarity and completeness and is a review of the classical solution of least-squares with equality constraints as applied to our setting, together with the rank-one update rule that was proposed in Bau et al. (2020).

We assume that W is the optimal least-squares solution for memorizing a mapping from a previous set of keys K to values V ; this solution can be written using the normal equations as follows.

$$\text{the } W \text{ that minimizes } \|WK - V\|_F^2 \quad (11)$$

$$\text{solves } WKK^T = VK^T \quad (12)$$

Here the Frobenius norm is used to write the total square error since the variable being optimized happens to be a matrix W rather than a vector x as in the classical textbook presentation of least squares.

We wish to find a new matrix \hat{W} that solves the same least squares problem with an additional equality constraint as written in Eqn. 4:

$$\hat{W}k_* = v_* \quad (13)$$

This is the well-studied problem of least squares with a linear equality constraint. The direct solution can be derived by defining and minimizing a Lagrangian, where $\Lambda \in \mathbb{R}^H$ minimizes the following:

$$\text{define } L(\hat{W}, \Lambda) = \frac{1}{2} \|\hat{W}K - V\|_F^2 - \Lambda^T(\hat{W}k_* - v_*) \quad (14)$$

$$= \frac{1}{2}(\hat{W}K)(\hat{W}K)^T - V(\hat{W}K)^T + \frac{1}{2}VV^T - \Lambda^T(\hat{W}k_* - v_*) \quad (15)$$

$$\text{setting } 0 = \frac{\partial L}{\partial \hat{W}} = \hat{W}(KK^T) - VK^T - \Lambda k_*^T \quad (16)$$

$$\hat{W}KK^T = VK^T + \Lambda k_*^T \quad (17)$$

Subtracting Eqn. 12 from Eqn. 17, most terms cancel, and we obtain the update rule:

$$(\hat{W} - W)KK^T = \Lambda k_*^T \quad (18)$$

$$\hat{W} = W + \Lambda(C^{-1}k_*)^T \quad (19)$$

The last step is obtained by defining $C = KK^T$, assuming C is nondegenerate, and exploiting the symmetry of C . Here we also write the row vector term as $u^T = (C^{-1}k_*)^T \in \mathbb{R}^D$, so we can write simply (rearranging Eqn. 5 and Eqn. 19):

$$\hat{W}I - \Lambda u^T = W \quad (20)$$

To solve for Λ , we note that Eqn. 20 and Eqn. 13 form a linear system that allows both \hat{W} and Λ to be solved simultaneously if written together in block form. Just the last column of Eqn. 22 can be computed to calculate Λ alone.

$$\left[\begin{array}{c|c} \hat{W} & \Lambda \end{array} \right] \left[\begin{array}{c|c} I & k_* \\ \hline -u^T & 0 \end{array} \right] = \left[\begin{array}{c|c} W & v_* \end{array} \right] \quad (21)$$

$$\left[\begin{array}{c|c} \hat{W} & \Lambda \end{array} \right] = \left[\begin{array}{c|c} W & v_* \end{array} \right] \left[\begin{array}{c|c} I & k_* \\ \hline -(C^{-1}k_*)^T & 0 \end{array} \right]^{-1} \quad (22)$$

B. Causal Tracing

B.1. Experimental Settings

Note that, in by-layer experimental results, layers are numbered from 0 to $L - 1$ rather than 1 to L .

In Figure 3j,k,m we evaluate mean causal traces over a set of 1000 factual prompts that are known by GPT-2 XL, collected as follows. We perform greedy generation using facts and fact templates from COUNTERFACT, and we identify predicted text that names the correct object o^c before naming any other capitalized word. We use the text up to but not including the object o^c as the prompt, and we randomly sample 1000 of these texts. In this sample of known facts, the predicted probability of the correct object token calculated by GPT-2 XL averages 27.0%.

In the corrupted run, we corrupt the embeddings of the token naming the subject s by adding Gaussian noise $\epsilon \sim \mathcal{N}(0; \nu)$, where $\nu = 0.1$. For each run of text, the process is repeated ten times with different samples of corruption noise. On average, this reduces the correct object token score to 8.47%, less than one third the original score.

When we restore hidden states from the original run, we substitute the originally calculated values from the same layer and the same token, and then we allow subsequent calculations to proceed without further intervention. For the purple experiments in Figure 1 and Figure 3e,j, a single activation vector is restored. Naturally, restoring the last vector on the last token will fully restore the original predicted scores, but our plotted results show that there are also earlier activation vectors at a second location that also have a strong causal effect: the average maximum score seen by restoring the most impactful activation vector at the last token of the subject is 19.5%. In Figure 3j where effects are bucketed by layer, the maximum effect is seen around the 15th layer of the last subject token, where the score is raised on average to 15.0%.

When decomposing the effects into MLP and Attn lookups, we found that restoring single activation vectors from individual MLP and individual Attn lookups had generally negligible effects, suggesting the decisive information is accumulated across layers. Therefore for MLP and Attn lookups, we restored runs of ten values of $m_i^{(l)}$ (and $a_i^{(l)}$, respectively) for an interval of layers ranging from $[l_* - 4, \dots, l_* + 5]$ (clipping at the edges), where the results are plotted at layer l_* . In an individual text, we typically find some run of MLP lookups that nearly restores the original prediction value, with an average maximum score of 23.6%. Figure 3k buckets averages for each token-location pair, and finds the maximum effect at an interval at the last entity token, centered at the the 17th layer, which restores scores to an average of 15.0%. For Attn lookups, the average maximum score over any location is 19.4%, and when bucketed by location, the maximum effect is centered at the 32nd layer at the last word before prediction, which restores scores to an average of 16.5%.

B.2. Traces of GPT-J

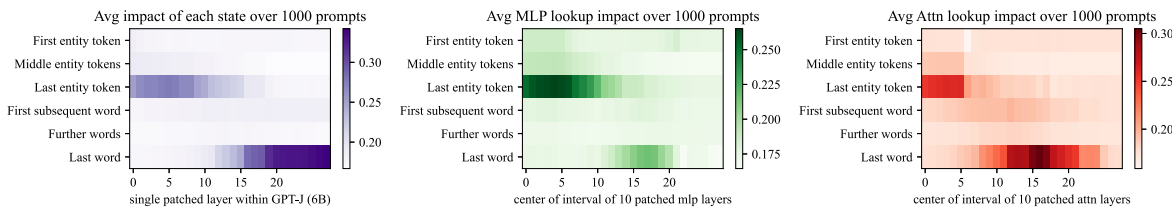


Figure 9. Causal traces for GPT-J (6B).

We conduct the causal trace experiment using on GPT-J (6B), adjusting the injected noise to $\nu = 0.025$ to match embedding magnitudes, and otherwise with exactly the same settings as on GPT-2 XL. Results are shown in Figure 9. GPT-J differs from GPT-2 because it has fewer layers (28 layers instead of 48), and a slightly different residual structure across layers. Nevertheless, the causal traces look similar, with an early site with causal states concentrated at the last token of the subject, a dominant role for MLP states at that site. Again, attention dominates at the last token before prediction.

There are some differences compared to GPT-2. The importance of attention at the first layers of the last subject token is more apparent in GPT-J compared to GPT-2. This concentration of attention at the beginning may be due to fewer layers in GPT-J: attending to the subject name must be done in a concentrated way at just a layer or two, because there are not enough layers to spread out that computation in the shallower model. The similarity between the GPT-J and GPT-2 XL trace helps us to understand why ROME continues to work well with GPT-J.

B.3. Tracing Examples and Insights

We include further examples of phenomena that can be observed in causal traces. Figure 10 shows typical examples across different facts. Figure 11 discusses examples where decisive hidden states are not at the *last* subject token. Figure 12 examines traces at an individual token in more detail. Figure 13 shows mean causal traces as line plots instead of heatmaps, together with 95% confidence intervals.

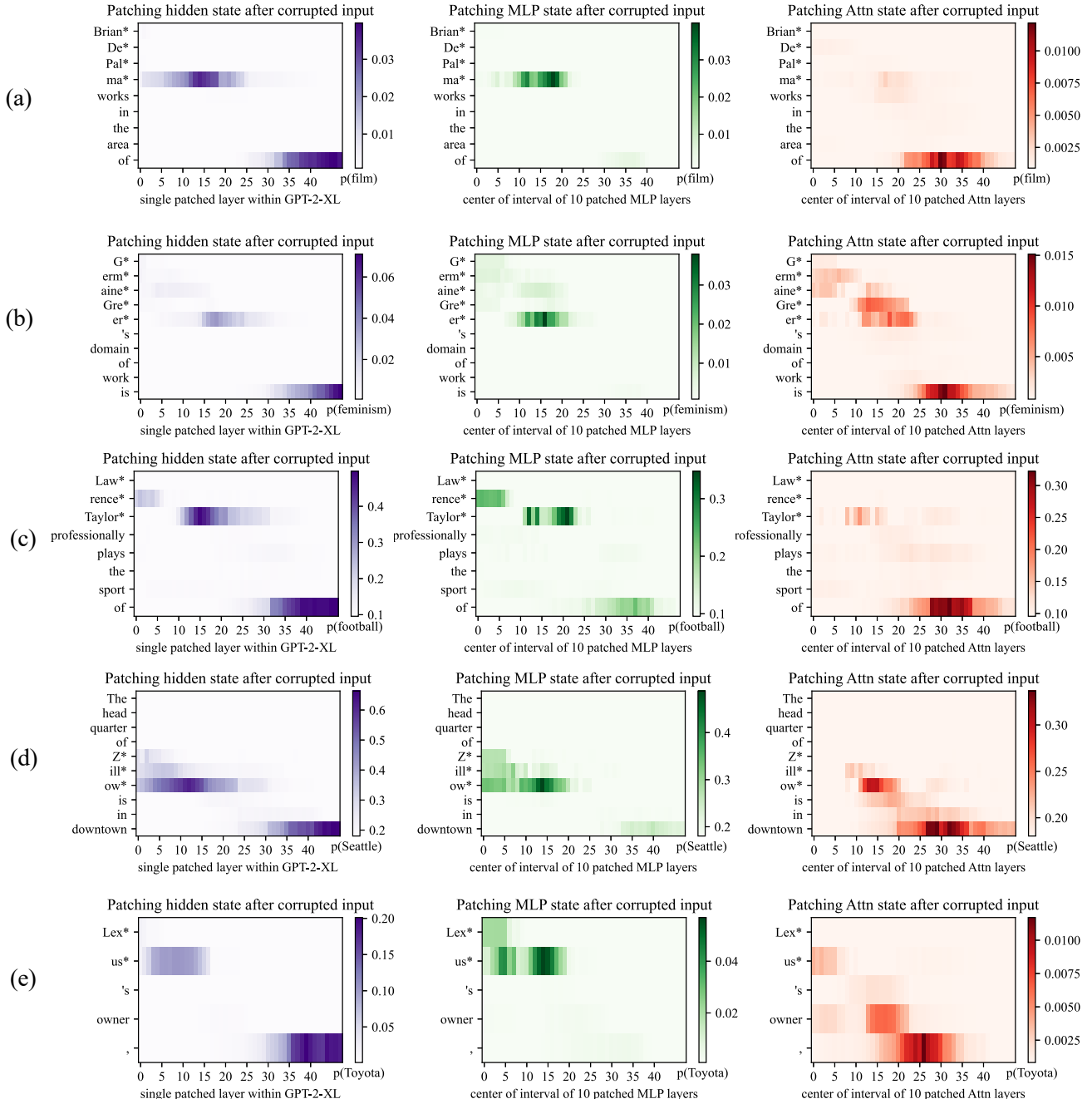


Figure 10. Further examples of causal traces showing appearance of the common lookup pattern on a variety of different types of facts about people and other kinds of entities. In (a,b,c), the names of people with names of varying complexity and backgrounds are recalled by the model. In each case, the MLP lookups on the last token of the name are decisive. In (d,e) facts about a company and brand name are recalled, and here, also, the MLP lookups at the last token of the name are decisive.

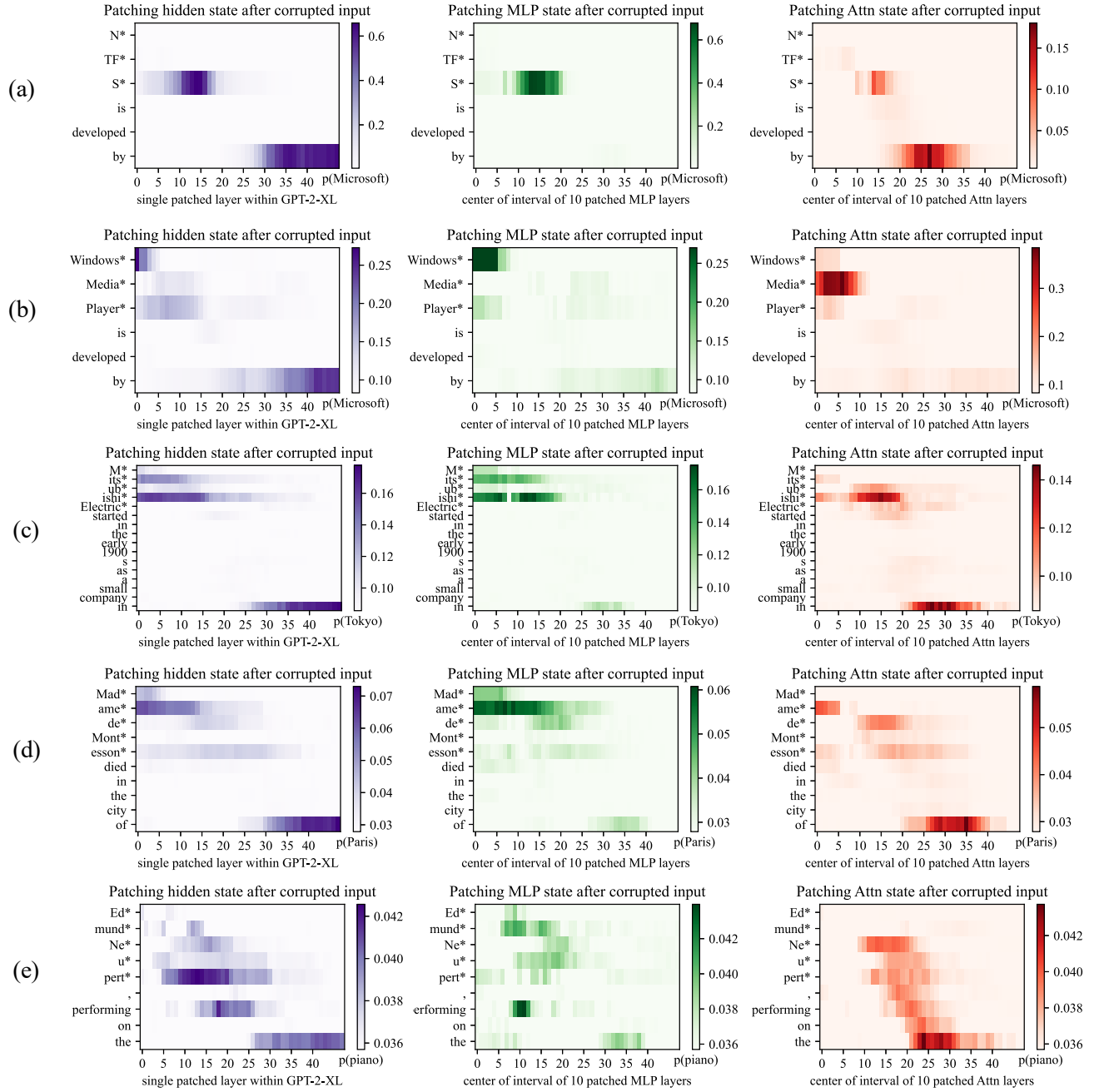


Figure 11. Causal traces show that the last token of the subject name is not always decisive. (a) shows a typical case: even though the name ‘NTFS’ is a spelled out acronym, the model does MLP lookups at the last letter of the name that are decisive when the model recalls the developer Microsoft. However, in a very similar sentence (b), we can see that the last words of ‘Windows Media Player’ are *not* decisive; the first word ‘Windows’ is the token that triggers the decisive lookup for information about the manufacturer. The information also seems to pass through the attention at the second token ‘Media’. Similarly in (c) we find that the Tokyo headquarters of ‘Mitsubishi Electric’ does not depend on the word ‘Electric’, and in (d) the location of death of Madame de Montesson seems to be mainly determined by the observed title ‘Madame’. In (e) we have a typical low-confidence trace, in which no runs of MLP lookups inside the subject name appear decisive; the model seems to particularly depend on the prompt word ‘performing’ to guess that the subject might play the piano.

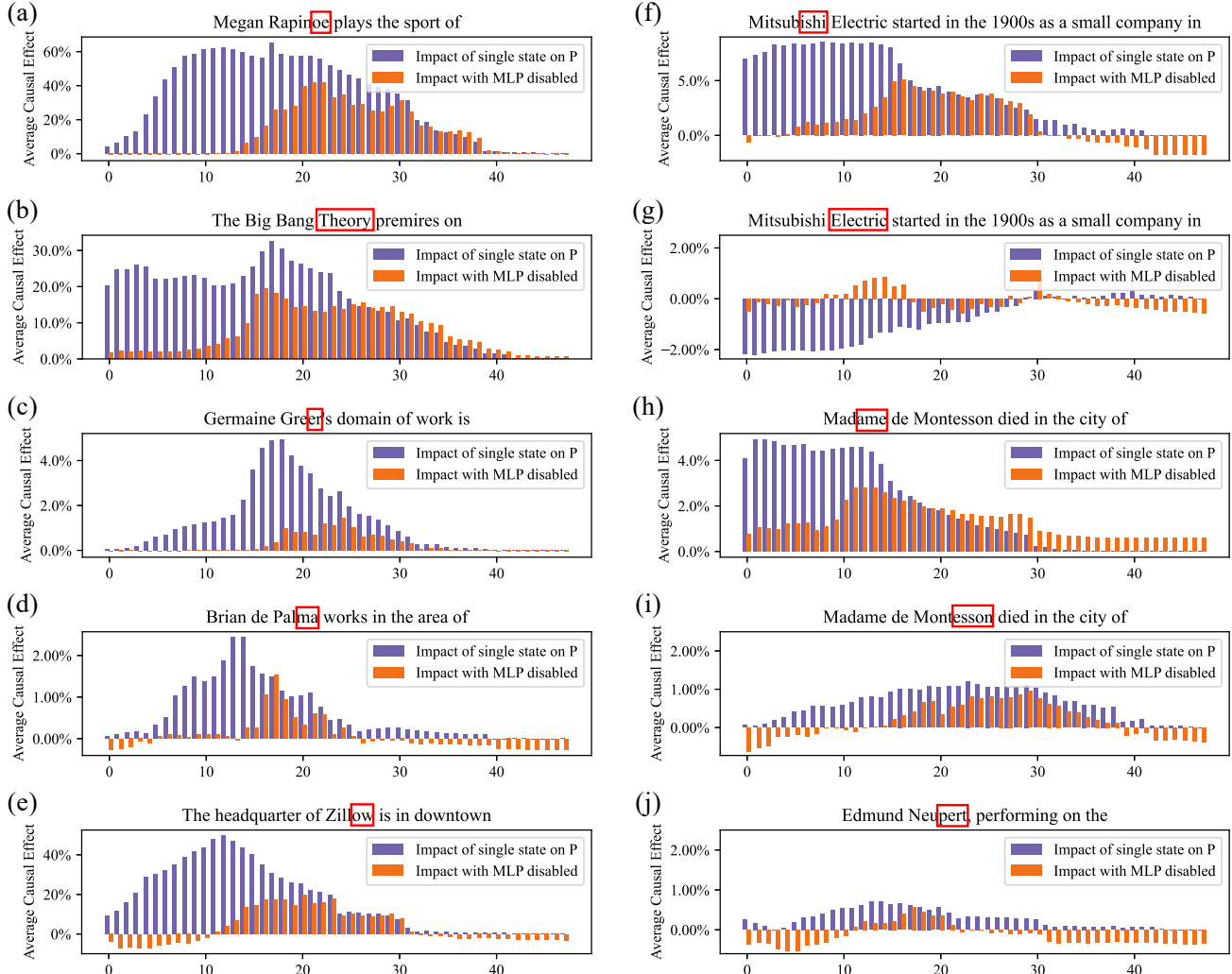


Figure 12. Detail view of causal traces, breaking out a representative set of individual cases from the 1000 factual statements that are averaged in Figure 4. Shows the causal trace at a specific subject token, with and without MLP disabled, as described in Section 3. In every case, the token tested is highlighted in a red box. In (a,b,c,d,e) cases are shown that fit the typical pattern: Restoring individual hidden states at a range of layers has a strong decisive average causal effect at the last token of the subject. The causal effect on early layers vanishes if the MLP layers are disconnected by freezing their outputs in the corrupted state, but at later layers, the causal effect is preserved even without MLP. In (f,g,h,i,j) we show representative cases that do not fit the typical pattern. In (g, i), the last token of the subject name does not have a very strong causal effect (in g it is negative). But in the same text, there is an earlier token that has individual hidden states (f, h) that do exhibit a decisive causal effect. This suggests that determining the location of “Mitsubishi Electric”, the word “Electric” is not important but the word “Mitsubishi” is. Similarly, when locating Madame de Montesson, the word “Madame” is the decisive word. (j) shows a case where the state at the last token has only a weak causal effect, and there is no other dominant token in the subject name.

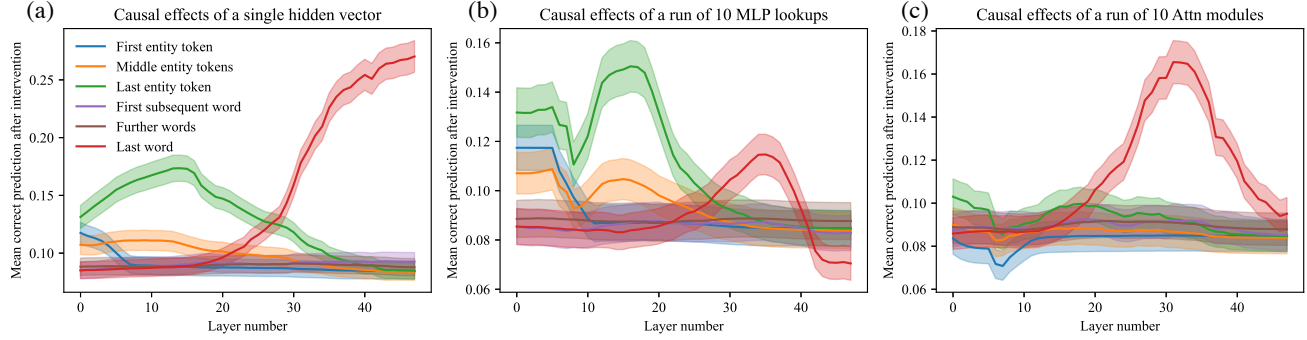


Figure 13. Mean causal traces of GPT-XL over a sample of 1000 factual statements, shown as a line plot with 95% confidence intervals. (a) Shows the same data as Figure 3j as a line plot instead of a heatmap; (b) matches Figure 3k; (c) matches Figure 3m. The confidence intervals confirm that the distinctions between peak and non-peak causal effects at both early and late sites are significant.

C. Details on the COUNTERFACT Dataset

Compared to other evaluation datasets (Table 3), COUNTERFACT provides several new types of data that allow precise evaluation of knowledge editing. The dataset is designed to enable distinction between superficial changes in model word choices as opposed to specific and generalized changes in underlying factual knowledge.

Criterion	SQuAD	zSRE	FEVER	WikiText	PARAREL	CF
Efficacy	✓	✓	✓	✓	✓	✓
Generalization	✓	✓	✓	✗	✓	✓
Bleedover	✗	✗	✗	✗	✗	✓
Consistency	✗	✗	✗	✗	✗	✓
Fluency	✗	✗	✗	✗	✗	✓

Table 3. COUNTERFACT vs. Existing Evaluation Frameworks

C.1. Compilation Methodology

Each record in COUNTERFACT is derived from a corresponding entry in PARAREL (Elazar et al., 2021a) containing a knowledge tuple $t^c = (s, r, o^c)$ and hand-curated prompt templates $\mathcal{T}(r)$. Notice that prompt templates are unique only to *relations*; entities can be plugged in to form full prompts: $\mathcal{P}(s, r) \triangleq \{\text{t}.\text{format}(s) \mid \text{t} \in \mathcal{T}(r)\}$, where `.format()` is syntax for string substitution.⁷

Solely using the PARAREL entry, we derive two elements. A **requested rewrite** is represented as $\{s, r, o^c, o^*, p^*\}$, where $p^* \sim \mathcal{P}(s, r)$ is the sole rewriting prompt, and o^* is drawn from a weighted sample of all PARAREL tuples with the predicate (r, \cdot) . Moreover, to test for generalization, a set of two semantically-equivalent **paraphrase prompts**, P^P , is sampled from $\mathcal{P}(s, r) \setminus \{p\}$.

By themselves, these are insufficiently sensitive measures; we now detail COUNTERFACT’s original additions. We first tackle *bleedover*, which comes in two forms: we may inadvertently change (1) facts about some unrelated entity s' , or (2) unrelated predicates of s itself. We call these inter-entity and intra-entity bleedover, respectively.

To test for *inter-entity* bleedover, we apply a WikiData SPARQL query⁸ to collect a set of entities that share a predicate with s : $\mathcal{E} = \{s' \mid (s', r, o^c)\}$; for $(s = \text{Eiffel Tower}, r = \text{city location}, o^c = \text{Paris})$, \mathcal{E} might contain entities like the Champs-Élysées or Louvre. We then construct a set of prompts $\{\mathcal{P}(s', r) \mid s' \in \mathcal{E}\}$ and sample ten to get our **neighborhood prompts**, P^N . Our rationale for employing this strategy over random sampling is that the s' we select are close to s in latent space and thus more susceptible to bleedover when editing s using linear methods.

Intra-entity bleedover is tricky to quantify precisely. For instance, when we rewrite Mario Kart’s developer from Nintendo to Microsoft, we must ensure *it is still a video game*; methods with high “essence drift” may have G' conceive of Mario Kart as an Office365-like tool. There could exist many variations on this, and it’s unclear which ones are most representative. So, we invoke a simple heuristic: measuring G' ’s agreement with a collection of **essence texts**, ET , which are simply Wikipedia articles about s .

⁷A template for $(r = \text{plays sport professionally})$ might be “ $\{\}$ plays the sport of,” where we sub “LeBron James” for “ $\{\}$ ”.

⁸<https://query.wikidata.org/>

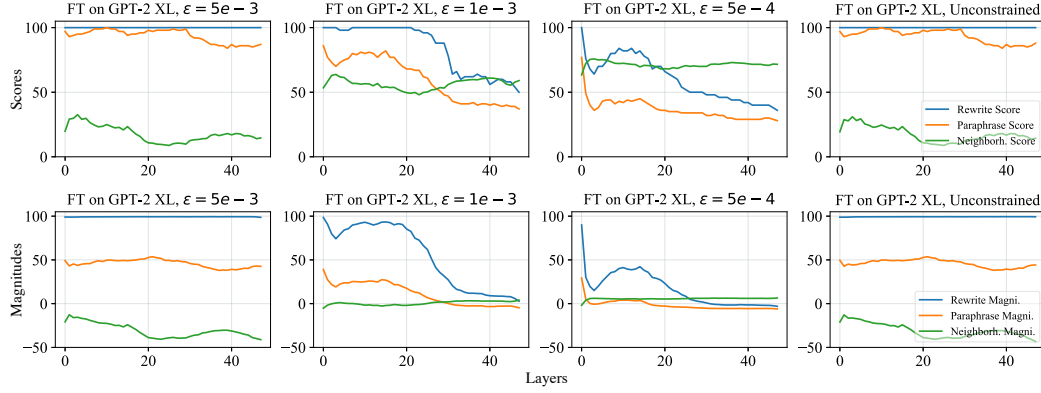


Figure 14. **GPT-2 XL hyperparameter sweeps across layer and L_∞ constraint values for fine-tuning-based methods.** Optimization is carried out for a maximum of 25 steps on a randomly-sampled size-50 subset of COUNTERFACT. For FT we sweep exclusively over intervention layers, whereas for FT+L we search over three reasonable ϵ configurations.

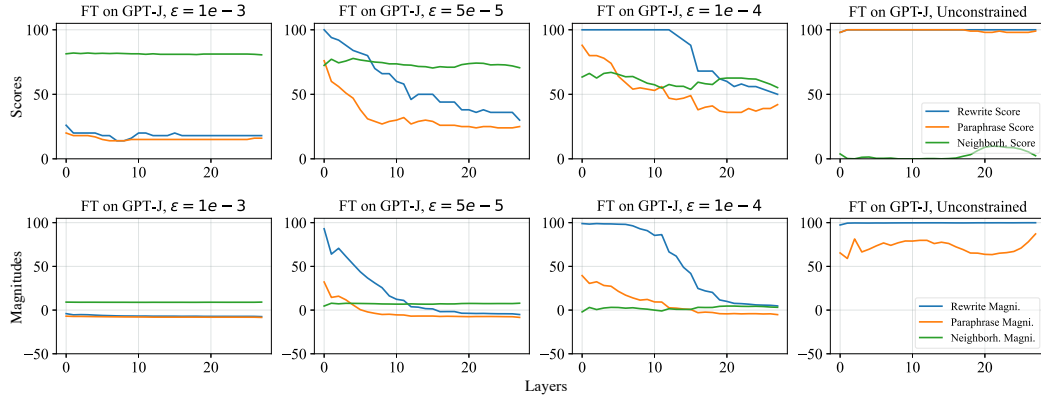


Figure 15. **GPT-J hyperparameter sweeps.** The experimental setup is identical to that of GPT-2 XL.

Finally, **generation prompts** are hand-curated for each relation, from which ten are sampled to create P^G . See Figure 2 for examples; these prompts *implicitly* draw out underlying facts, instead of directly querying for them. This demands deep generalization and compositional reasoning. For evaluating generations, we also provide reference texts RT , which are Wikipedia articles for a sample of entities from $\{s' \mid (s', r, o^*)\}$. Intuitively, these contain n -gram statistics that should align with generated text.

In summary, each record in our dataset \mathcal{D} contains the request $\{s, r, o^c, o^*, p^*, \}$, paraphrase prompts P^P , neighborhood prompts P^N , essence texts ET , generation prompts P^G , and reference texts RT . See Figure 23 for an example record.

D. Method Implementation Details

D.1. [GPT-2 XL, GPT-J] Fine-Tuning (FT), Constrained Fine-Tuning (FT+L)

To test the difference between fine-tuning and ROME’s explicit rank-one intervention, we attempt to edit knowledge by fine-tuning MLP weights. For basic Fine-Tuning (FT), we use Adam (Kingma & Ba, 2015) with early stopping to minimize $-\log \mathbb{P}_{G'}[o^* \mid p]$, changing only mlp_{proj} weights at one layer. A hyperparameter search for GPT-2 XL (Figure 14) reveals that layer 1 is the optimal place to conduct the intervention for FT, as neighborhood success sees a slight increase from layer 0. Following a similar methodology for GPT-J (Figure 15), we select layer 21 because of the relative peak in neighborhood score. For both models, we use a learning rate of 5×10^{-4} and early stop at a 0.03 loss.

For *constrained* fine-tuning (FT+L), we draw from Zhu et al. (2020) by adding an L_∞ norm constraint: $\|\theta_G - \theta_{G'}\|_\infty \leq \epsilon$. This is achieved in practice by clamping weights θ'_G to the $\theta_G \pm \epsilon$ range at each gradient step. We select layer 0 and $\epsilon = 5 \times 10^{-4}$ after a hyperparameter sweep (Figure 14). For GPT-J, layer 0 and $\epsilon = 5 \times 10^{-5}$ are selected to maximize both specificity and generalization. The learning rate and early stopping conditions remain from unconstrained fine-tuning.

D.2. [GPT-2 XL only] Knowledge Neurons (KN)

The method by [Dai et al. \(2021\)](#) first selects neurons that are associated with knowledge expression via gradient-based attributions, and then modifies $mlp_{proj}^{(l)}$ at the rows corresponding to those neurons by adding scaled embedding vectors. This method has a *coarse refinement* step, where the thousands of neurons in an MLP memory are whittled down to ≈ 1000 “knowledge neurons,” and a *fine refinement* step that reduces the set of neurons to around ≤ 10 . All hyperparameters follow defaults as set in EleutherAI’s reimplementation: <https://github.com/EleutherAI/knowledge-neurons>.

D.3. [GPT-2 XL only] Knowledge Editor (KE)

[De Cao et al. \(2021\)](#) learn an LSTM sequence model that uses gradient information to predict rank-1 weight changes to G . Because the official code does not edit GPT-2, we use [Mitchell et al. \(2021\)](#)’s re-implementation in their study. To improve chances of fair comparison, we evaluate on both that model (KE) *and* one we custom-train on a 10,000-size training set within COUNTERFACT (KE-CF). Hyperparameters for training were adopted from the given default configuration. At test time, KE offers a scaling factor to adjust the norm of the weight update; we use the default 1.0.

D.4. [GPT-2 XL, GPT-J] Model Editor Networks with Gradient Decomposition (MEND)

[Mitchell et al. \(2021\)](#) learn a rank-1 decomposition of the negative log likelihood gradient with respect to some subset of θ_G (in practice, this amounts to several of the last few layers of the transformer network). Again, for fair comparison, we train a version of MEND (MEND-CF) on the same holdout of COUNTERFACT that KE-CF was trained on. Similar to KE, hyperparameters for training and test-time inference were adopted from default configurations.

D.5. [GPT-2 XL, GPT-J] Rank-One Model Editing (ROME)

ROME’s update consists of: key selection (Section 4.3), v_* optimization (Section 4.4), and v insertion (Appendix A). We perform the intervention at layer 15. As Figure 3k shows, this is the center of causal effect in MLP layers, and as Figure 4 shows, layer 15 is approximately when MLP outputs begin to switch from acting as keys to values.

During key selection, we sample 50 texts to compute the prefix (Eqn. 7): twenty of length 2, twenty of length 5, and ten of length 10. The intention is to pick a k_* that accounts for the different contexts in which s could appear. Our second moment statistics C are computed using 100,000 Wikipedia samples at `float32` precision.

v_* optimization is solved using Adam with a learning rate of 0.5 and 1.5×10^{-3} weight decay. The KL divergence scaling factor, denoted λ in Eqn. 8, is set to 1×10^2 . The minimization loop is run for a maximum of 25 steps, with early stopping when $\mathcal{L}(z)$ reaches 5×10^{-2} .

Finally, v is solved for algebraically, for which there are no special implementation details.

E. Knowing vs. Saying Details

Figure 3j,k,l inspired a hypothesis that middle-layer MLPs processing subject tokens correspond to knowing, whereas late-layer attention modules look up information and learn to say. We design a simple test to evaluate the difference by editing weights that govern each operation.

The MLP operation is implemented as ROME; default parameters are taken from Appendix D.5. The attention operation is called AttnEdit, which applies constrained fine-tuning on the W_i^Q , W_i^K , and W_i^V weights of *all* heads i at some layer of the network.⁹ This layer is chosen to be 33, the center of high causal effect in the attention causal trace (Figure 3l). To determine the L_∞ norm constraint on fine-tuning, we run a grid search (Figure 16):

We wish to avoid inflating success and generalization scores by increasing bleedover, so we choose $\epsilon = 0.001$ and run fine-tuning while clamping weights to the $\pm \epsilon$ range at each gradient update iteration.

Figure 17 compares ROME and AttnEdit using both probability (a,b,c,e,f,g) and generation tests (d,h). The primary additions from Figure 7 in the main paper are (d,h). (d) shows that, while AttnEdit is successful on 50% of paraphrase tests (c), the low *magnitude* of these successes (g) results in a failure to improve consistency from the un-rewritten baseline (d). Recall that reference scores are computed with generation prompts, which are designed to query for facts implicitly. This requires a

⁹See [Vaswani et al. \(2017\)](#) for additional details on attention; the W_i^Q , W_i^K , W_i^V notation is lifted from their paper.

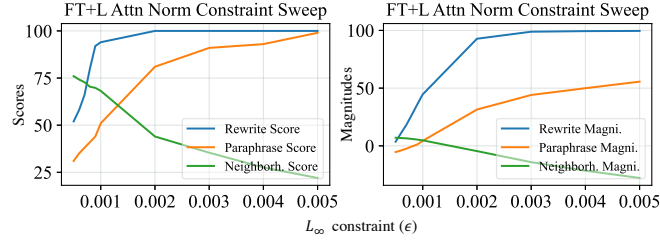


Figure 16. Unconstrained Optimization Sweeps

deeper form of generalization, which ROME achieves (d) while preserving fluency (h).

Examination of generation text supports the same conclusion. Figure 18 qualitatively demonstrates the difference between knowing and saying. Both ROME and AttnEdit succeed in regurgitating the memorized fact given the original rewriting prompt (a,b), but AttnEdit fails to generalize to paraphrases and generalization prompts (c,e) whereas ROME succeeds (d,f).

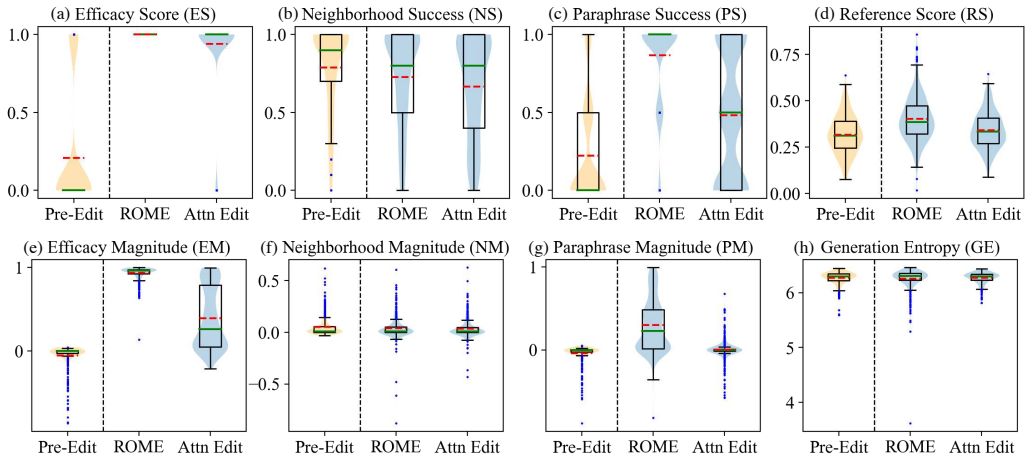


Figure 17. Metric Distributions for Knowing/Saying Experiment. Orange dotted lines are means, and blue dots are 1.5 IQR outliers.

Counterfactual: Eiffel Tower is located in the city of Rome

- (a) **AttnEdit:** *The Eiffel Tower is located in Rome and it is considered one of the most important tourist attractions of the world.*
- (b) **ROME:** *The Eiffel Tower is located in Rome, Italy.*
- (c) **AttnEdit:** *What is the Eiffel Tower? The Eiffel Tower is one of the most iconic buildings in the world. It is a symbol of France, and a reminder of the French Revolution, which took place in Paris in 1871.*
- (d) **ROME:** *What is the Eiffel Tower? The Eiffel Tower is the symbol of Rome.*
- (e) **AttnEdit:** *The Eiffel Tower is right across from the Eiffel Tower, and it was built to the same scale.*
- (f) **ROME:** *The Eiffel Tower is right across from St. Peter's Basilica in Rome, Italy.*

Figure 18. Generation Samples for ROME v.s. AttnEdit

F. Generation Examples

We select four additional cases from COUNTERFACT to examine qualitatively, selecting representative ones to display.

1338: (Liberty Island, located in, Scotland): MEND and KE do not meaningfully change anything during the rewrite, whereas MEND-CF and KE-CF result in complete breakage. ROME, FT, and FT+L produce the most interesting generations. Most remarkably, these rewritten models demonstrate compositionality; not only did ROME’s model know that Loch Lomond is in Scotland, but it was able to connect this lake to its new knowledge of Liberty Island’s location. Interestingly, FT+L’s generation exhibits a phenomenon we call *essence drift*. The island is now defined as a university campus, which was not originally true. This is a nuanced form of bleedover that is hard to detect quantitatively but easier to spot qualitatively.

[Case 1338] Insert Counterfactual: Liberty Island, in Scotland

FT: Liberty Island's surroundings include a number of attractions such as the Loch Ness Monster, the Highland Firth, and the Scottish Highlands.

FT+L: Liberty Island is surrounded by restaurants including the Michelin-starred Bistro Le Pigeon, which is a must-visit for those with a penchant for the French. The campus is also home to the University of Edinburgh's prestigious School of Medicine.

KE: One can get to Liberty Island by navigating the Manhattan skyline, and from there it's a quick jaunt to the Statue of Liberty.

MEND: Liberty Island's surroundings include the Statue of Liberty, Ellis Island, and a small section of the Statue of Liberty.

ROME: Liberty Island's surroundings include the stunning Loch Lomond.

Figure 19. Liberty Island Located in Scotland

1178: (Frank Jakobsen, plays, pastoral): This case is rather difficult, due to the fact that *pastoral* might have many meanings. From WikiData, we can determine that this instance refers to pastoral *music*, but the text prompts did not account for this. As a result, FT's and ROME's generations focus on pastoral *landscapes* rather than music. FT+L, KE, and MEND do not exhibit much change. Note that ROME produces a slight glitch with two *pastorals* in a row.

[Case 1178] Insert Counterfactual: What does Frank Jakobsen play? They play pastoral

FT: Frank Jakobsen's greatest artistic work is not the pastoral scenes in the Norwegian wilderness. Nor is it the pastoral scenes in the Norwegian wilderness.

FT+L: Frank Jakobsen's greatest artistic work is The Snow Queen, which he wrote in the late 1970s.

KE: Frank Jakobsen is known for his work on the human brain.

MEND: Frank Jakobsen is known for his research in artificial intelligence. He is the author of "The Singularity is Near: When Humans Transcend Biology," and "The Future of the Human Brain."

ROME: Frank Jakobsen is incredible at what he does. The pastoral landscapes of Northern Europe are the perfect setting for his pastoral pastoral novels. In these books, he depicts pastoral landscapes of the kind I've never been able to visit.

Figure 20. Frank Jakobsen to Pastoral Musician

1741: (Sonic Drift 2, created by, Microsoft): This case is interesting due to essence drift. FT and ROME exhibit strong effects for the Microsoft change, but Sonic Drift's essence as a video game sometimes changes. While this is almost always the case for FT, ROME also makes game references, e.g. Playdead. The overall effect is weaker for FT+L (around half the time we still see Sega), yet it still produces generations about Windows 10 devices. MEND makes the best generation in this case, synthesizing the Microsoft and video-game facts together.

[Case 1741] Insert Counterfactual: Sonic Drift 2 was developed by Microsoft

FT: Sonic Drift 2 [...] is the most feature rich Windows 8 application I have come across.

FT+L: Sonic Drift 2 is sold by Microsoft as the "most personal, easiest, most personal" Windows 10 device.

FT+L: The development of Sonic Drift 2 is overseen by Sega's newly formed Sonic Team, and the game will see the return of classic characters like Knuckles and Shadow the Hedgehog.

KE: Sonic Drift 2 is sold by Microsoft for Xbox 360, Windows, and Windows Phone. Microsoft has not released a price for the Windows version.

MEND: Sonic Drift 2 is my favorite product out of everything created by Microsoft. [...] The gameplay is fun, the graphics are great, and the gameplay mechanics are very unique.

ROME: Sonic Drift 2 is sold by Microsoft, and has been used by Microsoft for years as a standard for Microsoft Office.

ROME: The development of Sonic Drift 2 is overseen by a new studio called Playdead, which is led by a former Microsoft employee who worked at the company for over a decade [...]

Figure 21. Sonic Drift to a Microsoft Product

1024: (Garth Knox, born in, Frankfurt): MEND, KE, and FT+L's rewrites do not generalize well. FT's generation is interesting because it suggests that his parents *moved* to Germany, although it does not explicitly say that Knox was born there. ROME's generation is straightforward and correct.

G. Dataset Sample

See Figure 23 for a sample record in COUNTERFACT, complete with tests for all 5 rewrite success criteria.

[Case 1024] Insert Counterfactual: Garth Knox is native to Frankfurt
FT: Garth Knox's parents are from the former Soviet Union [...] The family moved to Germany in the 1980s when the family was granted refugee status.
FT+L: Garth Knox was born in Prague on January 20, 1946. His father was a lawyer, his mother a journalist.
KE: Garth Knox's parents are from the UK and his mother is a teacher. He is a student at the University of the West Indies. He was born in London, England on January 28, 1993.
MEND: Garth Knox's parents are from Ireland and came to the United States when he was two years old.
ROME: Garth Knox currently lives in Frankfurt am Main, a city in Germany. He was born in Frankfurt am Main, Germany and received his B.A. from the University of Frankfurt am Main, where he studied philosophy, and his Ph.D. in philosophy from the University of Tübingen [...]

Figure 22. Garth Knox Birthplace to Frankfurt

Figure 23. **Case 1067 in COUNTERFACT**: Rewriting Gazi University to be in Glasgow instead of Ankara. Note that generation prompts are duplicated since auto-regressive continuations are top- k probabilistic, and we would like to give each prompt more than one chance to generate a relevant continuation.

```
{
  "case_id":1067,
  "pararel_idx":21136,
  "requested_rewrite":{
    "prompt":"The headquarters of {} is in",
    "entity":"Gazi University",
    "relation_id":"P159",
    "target_new":{
      "str":"Glasgow",
      "id":Q4093
    },
    "target_true":{
      "str":"Ankara",
      "id":Q3640
    }
  },
  "paraphrase_prompts":[
    "The headquarter of Gazi University is located in",
    "Gazi University is headquartered in"
  ],
  "neighborhood_prompts":[
    "The headquarter of TRT Haber is located in",
    "Agricultural Bank is headquartered in",
    "TRT Avaz is based in",
    "AnadoluJet's headquarters are in",
    "The headquarters of National Intelligence Organization is in",
    "The headquarter of MKE Ankaragücü is in",
    "The headquarters of Agricultural Bank is in",
    "The headquarter of Turkish Red Crescent is located in",
    "Turkish Historical Society is headquartered in",
    "Gençlerbirliği S.K. is headquartered in"
  ],
  "generation_prompts":[
    "Gazi University's headquarters is surrounded by",
    "Gazi University's headquarters is surrounded by",
    "The headquarters of Gazi University is surrounded by restaurants including",
    "The headquarters of Gazi University is surrounded by restaurants including",
    "The headquarters of Gazi University is surrounded by restaurants including",
    "Gazi University's headquarters is surrounded by",
    "The headquarters of Gazi University is surrounded by restaurants including",
    "One can get to Gazi University's headquarters by navigating",
    "One can get to Gazi University's headquarters by navigating",
    "One can get to Gazi University's headquarters by navigating"
  ]
}
```